# A STING-dependent innate sensing pathway mediates resistance to corneal HSV-1 infection via upregulation of the antiviral effector tetherin

**D.J. Royer, D.J.J. Carr[1,2]**

[1]Departments of Microbiology & Immunology and [2]Ophthalmology,

The University of Oklahoma Health Sciences Center, Oklahoma City, OK USA.

**Corresponding Author:** Daniel J.J. Carr

Address: Department of Ophthalmology, DMEI Acers Pavilion, Room 415,

608 Stanton L. Young Blvd., Oklahoma City, OK 73104

Phone: 405-271-8784

E-mail: Dan-Carr@ouhsc.edu

**Disclosure:** the authors have no financial or commercial conflicts of interest

**Running title:** STING drives interferon to tether HSV-1

## ABSTRACT

Type 1 interferons (IFNα/β) mediate immunologic host resistance to numerous viral infections including herpes simplex virus type 1 (HSV-1). The pathways responsible for maintenance of IFNα/β signaling during the innate immune response to acute HSV-1 infection in the cornea are incompletely understood. Using a murine ocular infection model, we hypothesized that the stimulator of IFN genes (STING) mediates host resistance to HSV-1 infection in the external ocular surface and preserves the structural integrity of this immune-privileged mucosal site. Viral pathogenesis, tissue pathology, and host immune responses during ocular HSV-1 infection were evaluated and characterized by plaque assay, esthesiometry, pachymetry, immunohistochemistry, flow cytometry, and siRNA transfection in wildtype C57BL/6 (WT), STING-deficient ($STING^{-/-}$), and IFNα/β receptor-deficient ($CD118^{-/-}$) mice at days 3-5 post infection (pi). The presence of STING was critical for sustained control of HSV-1 replication in the corneal epithelium and neuroinvasion, but loss of STING had a negligible impact with respect to gross tissue pathology. Auxiliary STING-independent IFNα/β signaling pathways were responsible for maintenance of the corneal integrity. Lymphatic vessels, mast cells, and sensory innervation were compromised in $CD118^{-/-}$ mice concurrent with increased tissue edema. STING-dependent signaling led to the upregulation of tetherin, a viral restriction factor we identify to be important in containing the spread of HSV-1 *in vivo*.

## INTRODUCTION

Viral infections set off cellular alarms through the detection of pathogen-associated molecular patterns (PAMPs). Virus-derived PAMPs are recognized by a variety of innate sensors that operate through distinct signaling pathways to upregulate IFNα/β and stimulate NF-κB-driven cytokine production.[1] IFNα/β secretion mediates canonical autocrine and paracrine signaling through the IFNα/β receptor (CD118). The IFNα/β signaling pathway modulates hundreds of IFN-stimulated genes (ISGs), the products of which activate immunologic countermeasures and promote host resistance to viral infections.[2] Specific host-pathogen interactions ultimately dictate the effectiveness of IFNα/β signaling, as many viruses including HSV-1 employ numerous mechanisms to evade, counteract, or otherwise disrupt pathway components or downstream ISGs.[3,4]

Multiple pattern recognition receptor families can initiate IFNα/β signaling during DNA virus infections.[5–7] The pathways by which HSV-1-derived PAMPs mediate IFNα/β induction and host resistance within mucosal sites are incompletely understood. Our lab has previously shown that loss of toll-like receptor (TLR) signaling does not enhance HSV-1 pathogenesis in the cornea; rather, a TLR-independent pathway involving the STING-dependent DNA sensor IFI16 (IFN inducible protein 16) initiates host resistance to HSV-1 in the corneal epithelium.[8] STING operates as a direct sensor of cytosolic DNA and a central signaling adaptor protein for an array of cytoplasmic and nuclear DNA sensors.[6,9] STING-dependent induction of IFNα/β involves activation of the transcription factor IFN regulatory factor 3 (IRF3) via phosphorylation by TANK-binding kinase

1 (TBK1).[10] IFI16 has been linked to early IFNβ production in HSV-1-infected monocyte/macrophage cell lines, fibroblasts, and in the corneal epithelium.[8,11,12] However, IFI16 is degraded by the HSV-1 early gene product ICP0, suggesting that the STING-TBK1-IRF3 signaling axis is essential for early detection of viral infection but may be subsequently counteracted by the virus.[11,13,14] We investigated the role of STING in sustained IFNα/β signaling in a mouse model of ocular HSV-1 infection, and hypothesized that STING mediates innate host resistance to corneal HSV-1 infection and preserves the corneal integrity through day 5 pi.

Currently, there are no prophylactic or therapeutic vaccines licensed to prevent sequelae elicited by HSV-1 infection.[15] These medically relevant pathologies span in severity from intermittent mucocutaneous lesions (*i.e.* oral and genital herpes, herpetic keratitis) to neurological damage and corneal blindness.[16] The cornea is a delicate mucosal site, and pathological alteration of the tissue architecture hinders visual acuity. Recurrent corneal HSV-1 infection contributes to a variety of pathological sequelae in the human cornea that can affect visual acuity and health of the ocular surface including edema, scarring, neovascularization, and loss of sensation.[15,17]

Our investigation highlights the subtleties of IFNα/β-signaling pathways in promoting resistance to ocular HSV-1 infection. Resistance to HSV-1 involves the coordinated activities and interactions of many cell types and structures in the cornea to detect the viral infection, limit local replication, and impede spread to peripheral nerve ganglia. Our findings collectively identify that the STING

signaling axis is critical for host resistance to corneal HSV-1 infection through a mechanism involving the viral restriction factor tetherin (also known as BST2, CD317, HM1.24, PDCA-1). A wealth of evidence supports tetherin as a viral restriction factor active against a diverse range of enveloped viruses *in vitro* and *in vivo* by impeding cell-cell spread of nascent virions.[18–20] We show that tetherin limits HSV-1 replication in the corneal epithelium and impedes viral dissemination to the nervous system.

## RESULTS

### STING promotes sustained resistance to HSV-1 replication in the eye

To identify the impact of STING relative to acute HSV-1 infection of the ocular surface, HSV-1 infection of the cornea was modeled using wild type (WT) C57BL6/J, STING-deficient ($STING^{-/-}$), and highly susceptible IFNα/β receptor-deficient ($CD118^{-/-}$) mice. By day 5 post infection (pi), $STING^{-/-}$ and $CD118^{-/-}$ mice harbored significantly more infectious virus in the cornea than WT mice (Figure 1a). A moderate increase in titer comparing $CD118^{-/-}$ mice to $STING^{-/-}$ mice was also observed (Figure 1a). This data indicates that the STING-signaling pathway is a major determinant of IFNα/β-dependent host resistance within the cornea following HSV-1 infection.

### STING deficiency does not exacerbate acute corneal pathology

Corneal sensation and edema were measured following HSV-1 infection via Cochet-Bonnet esthesiometry and ultrasound pachymetry, respectively. WT mice had no appreciable changes in corneal sensation (Figure 1b) relative to

healthy controls (not shown) by day 5 pi, though significant sensation loss and corneal denervation is observed in WT mice by day 8 pi using this experimental model.[21] In contrast, CD118$^{-/-}$ mice exhibited hyperacute corneal sensation loss such that the pressure required to elicit a blink response was 15 g/mm$^2$ higher than WT by day 5 pi (Figure 1b).

Despite the similar magnitude of infectious virus recovered from the corneas of STING$^{-/-}$ and CD118$^{-/-}$ mice, corneal sensation loss relative to WT was not observed in STING$^{-/-}$ mice through day 5 pi (Figure 1b). Corneas of CD118$^{-/-}$ mice were more edematous than either STING$^{-/-}$ or WT mice by day 3 pi (Figure 1c). The severity of corneal edema continued to worsen in CD118$^{-/-}$ mice through day 5 pi, while differences in corneal thickness observed in WT and STING$^{-/-}$ mice following infection were generally unremarkable compared to baseline uninfected (UI) controls (Figure 1c). Moreover, the mechanism underlying HSV-1 associated corneal sensation loss is likely dependent on intrinsic cell-signaling pathways and is not merely attributable to infection of the sensory neurons, as STING$^{-/-}$ and CD118$^{-/-}$ mice harbored 100-1000 times more infectious virus in the TG than WT by day 5 pi (data not shown; $p \leq 0.001$).

**STING promotes host resistance in the corneal epithelium and restrains HSV-1 neuroinvasion**

Confocal imaging was employed to visualize the localization of HSV-1 antigen in cornea whole mounts at day 5 pi. Viral lesions were geographically isolated in WT corneas, whereas diffuse HSV-1 labeling was observed in STING$^{-/-}$ and CD118$^{-/-}$ corneas (Figure 1d). High-magnification confocal analysis of the

viral lesions revealed that HSV-1 antigen is present almost exclusively in the outermost epithelial layers of WT and STING$^{-/-}$ corneas but penetrates into the deeper stromal layers of CD118$^{-/-}$ corneas (Figure 1e).

The pathogenesis of HSV-1 involves neuroinvasion and retrograde dissemination to the tissue-innervating trigeminal ganglion (TG) following infection of the oculo-orofacial mucosae. Subbasal sensory nerve fibers of TG neurons innervate the corneal epithelium and enable direct epithelial-nerve spread of HSV-1.[21] CD118$^{-/-}$ and STING$^{-/-}$ mice harbored 100 times more infectious HSV-1 in the TG than WT as early as day 3 pi (Supplemental Figure 1a), indicating that STING-mediated signaling restricts dissemination of HSV-1 from the corneal epithelium to the nervous system.

**STING deficiency leads to a minimal reduction in ISG expression**

We hypothesized that the STING signaling axis drives and sustains IFNα/β production in the cornea following HSV-1 infection. To investigate this hypothesis, a modest gene array was utilized to measure downstream ISGs at day 5 pi. Cluster image mapping (Figure 2a) and quantification (Figure 2b) of compiled data show comparatively similar profiles for WT and STING$^{-/-}$ mice and a paucity of transcript expression in CD118$^{-/-}$ mice with respect to genes upregulated by IFNα/β-signaling. Still, other genes are repressed by IFNα/β signaling[22] such as Wars, which exhibits higher expression in the CD118$^{-/-}$ group than in WT or STING$^{-/-}$ samples (Figure 2b).

Statistical analysis divulged a reduction in transcript expression comparing STING$^{-/-}$ to WT mice for Bst2, Irf3, Irf9, Oas2, Oas3, and Rnasel (Figure 2b). Of

these, the viral restriction factor Bst2 (tetherin) was the only transcript identified with pronounced margins of differential expression. Tetherin was highly upregulated in WT corneas yet expression was nearly 10 times lower in STING$^{-/-}$ and CD118$^{-/-}$ corneas (Figure 2b), consistent with the observed differences in viral pathogenesis in our model (Figure 1a). Despite being statistically significant, expression differences in the other genes of interest were less impressive and not pursued.

**Amplified myeloid cell recruitment is observed in STING deficient mice**

To uncover the immunologic mechanisms responsible for STING-dependent resistance to HSV-1 in the cornea, infiltrating leukocytes and cytokine concentrations were investigated. Flow cytometry was used to evaluate and characterize the cornea-infiltrating myeloid cells at day 5 pi. STING$^{-/-}$ mice had nearly twice as many total infiltrating myeloid cells (CD45$^{+}$ CD11b$^{+}$) as WT mice (Figure 3a). Confocal microscopy used to confirm uniform distribution of CD11b$^{+}$ cells throughout cornea flat mounts at day 5 pi for all three genotypes (data not shown). WT and CD118$^{-/-}$ mice had comparable total numbers of infiltrating myeloid cells (Figure 3a). Ly6C and Ly6G antigens were used to distinguish monocytes and neutrophils (PMN). No statistical difference was measured in the total number of cornea-infiltrating Ly6C$^{low}$ Ly6G$^{hi}$ PMN comparing WT, STING$^{-/-}$, and CD118$^{-/-}$ mice, although there was a propensity for the proportion of PMN to be elevated in CD118$^{-/-}$ mice (Figure 3b).

Differences were observed in Ly6C$^{+}$ cornea-infiltrating monocytes at day 5 pi. We identified two distinct Ly6C$^{+\,(mid\text{-}high)}$ monocyte populations comprising

177 Ly6G$^{high}$ (Figure 3c) and Ly6G$^{low}$ (Figure 3d) subsets. The ratio of the Ly6G$^{high}$ to
178 Ly6G$^{low}$ monocyte subsets was also evaluated (Figure 3e). The Ly6C$^{+}$ Ly6G$^{low}$
179 monocyte population is largely absent in the corneas of CD118$^{-/-}$ mice (Figure 3d)
180 consistent with their identity as inflammatory monocytes, which serve as innate
181 sentinels against HSV-1.[23] Representative dot plots are shown for WT, STING,
182 and CD118$^{-/-}$ mice (Figure 3f). A higher ratio of Ly6C$^{+}$ Ly6G$^{high}$ monocytes was
183 observed in the CD118$^{-/-}$ corneas compared to STING$^{-/-}$ or WT groups (Figure
184 3e), and a higher total number of Ly6C$^{+}$ Ly6G$^{high}$ monocytes were present in the
185 corneas of STING$^{-/-}$ mice than in other groups.

186 Despite the high number of inflammatory monocytes (Ly6C$^{+}$ Ly6G$^{low}$)
187 recruited into the corneas of STING$^{-/-}$ mice, HSV-1 replication in the epithelium is
188 not controlled (Figure 1a,e). However, gross tissue edema (Figure 1c) and viral
189 penetration into the stroma (Figure 1e) are prevented in STING$^{-/-}$ mice, which we
190 attribute in part to the antiviral effects of inflammatory monocyte infiltration.
191 Protein concentrations of IFN$\alpha_{2,4}$ and IFNγ in STING$^{-/-}$ corneas were comparable
192 to or exceeded WT at day 5 pi (Figure 3g), thus substantiating the ISG array
193 findings (Figure 2). No elevation in IFN$\alpha_{2,4}$ concentrations were observed in WT
194 or STING$^{-/-}$ corneas relative to UI at day 3 pi (not shown). Concentrations of the
195 monocyte chemotactic C-C motif chemokine ligands CCL2 and CCL20 were
196 elevated in STING$^{-/-}$ corneas at day 5 pi (Figure 3h), thus providing a mechanistic
197 explanation for the observed enhancement in monocyte infiltration.[23,24]
198 Production of the proinflammatory cytokines IL-1β and IL-17 were also measured

(Figure 3i), but the concentrations detected did not correlate with severity of tissue pathology or viral pathogenesis.

In order to rule out a potential functional defect in the inflammatory monocytes in STING$^{-/-}$ mice, CD11b$^{+}$ splenocytes were isolated from uninfected WT or STING$^{-/-}$ mice and inoculated *in vitro* with HSV-1 at various multiplicities of infection (MOI). Supernatant virus titers did not differ between WT and STING$^{-/-}$ CD11b$^{+}$ splenocyte cultures observed at 24 hours pi (Supplemental Figure 2a). By 48 hours pi, similar findings were observed in culture supernatants with a subtle variance at 1 MOI in which there was a modest but statistically significant increase in HSV-1 recovered from the infected CD11b$^{+}$ STING$^{-/-}$ cell cultures (Figure 3j).

Prior to isolation of CD11b$^{+}$ cells, splenocytes isolated from healthy WT and STING$^{-/-}$ mice had a similar distribution of CD45$^{+}$ CD11b$^{+}$ myeloid cell subsets based on Ly6C and F4/80 antigen expression (Supplemental Figure 2b). CD11b$^{+}$ splenocytes cultured for 24 hours showed no differences in the relative proportions of F4/80$^{+}$ Ly6C$^{-}$ macrophages or F4/80$^{+}$ Ly6C$^{mid\text{-}high}$ monocytes in the presence or absence of HSV-1 (Supplemental Figure 2c,d). Consistent with previous findings,[25] macrophages isolated from STING$^{-/-}$ mice exhibited a deficit in major histocompatibility class II (MHC II) upregulation relative to WT in HSV-1 infected cultures (Supplemental Figure 2d). However, MHC II expression profiles were similar in both WT and STING$^{-/-}$ monocyte subsets (Supplemental Figure 2c,d), thereby providing no phenotypic indication of functional defects in STING$^{-/-}$ monocytes.

**Peri-corneal lymphatic vessels and mast cells are lost in CD118$^{-/-}$ mice**

Corneal neovascularization and/or impairment of the peri-corneal vasculature were examined to further characterize differences in acute ocular pathology following HSV-1 infection. Blood and lymphatic vessels were labeled using anti-CD31 and anti-Lyve-1 antibodies, respectively, to visualize the peri-corneal vasculature at day 5 pi (Figure 4a). The vasculature of STING$^{-/-}$ mice resembled WT (Figure 4a). Neovascularization was modest in the WT and STING$^{-/-}$ mice and notably absent in the CD118$^{-/-}$ animals by day 5 pi (Figure 4a) relative to healthy UI corneas (not shown). The peri-corneal blood vessels remaining in CD118$^{-/-}$ mice were distended relative to those seen in STING$^{-/-}$ or WT mice (Figure 4a) consistent with observations of enhanced tissue edema in CD118$^{-/-}$ mice (Figure 1c). Moreover, a profound loss of the lymphatic vasculature is observed in CD118$^{-/-}$ mice by day 5 pi (Figure 4a).[26]

Tissue-resident mast cells associated with the peri-corneal vasculature were also investigated at day 5 pi due to their pleiotropic immunomodulatory capacity[27] and protective role against ocular HSV-1 infection.[28] Mast cells were identified by avidin staining and found in the limbal aspect of the corneas of WT and STING$^{-/-}$ mice as previously described.[28] In stark contrast, mast cells were lost in the corneas of CD118$^{-/-}$ mice by day 5 pi (Figure 4b). We speculate the pathological corneal edema observed in CD118$^{-/-}$ mice results from multiple mechanisms including: penetration of HSV-1 into the stroma, lymphatic vessel destruction, and loss of mast cells.

**STING is required for tetherin expression in the corneal epithelium**

A direct STING-dependent mechanism responsible for containment of viral replication and dissemination remained to be identified. Due to its expression profile in the ISG array, the viral restriction factor tetherin was explored as a candidate in controlling HSV-1 in the corneal epithelium. We hypothesized that tetherin impedes spread of HSV-1 in the cornea in a STING-dependent manner. Immunolabeling in WT, STING$^{-/-}$, and CD118$^{-/-}$ corneas at day 5 pi was utilized to identify the presence and localization of tetherin (Figure 4c). Tetherin colocalized with the CD31$^{+}$ blood vessels in all groups. In contrast, high levels of tetherin protein expression was observed in the corneal epithelium of WT but not STING$^{-/-}$ or CD118 mice$^{-/-}$ (Figure 4c). Tetherin expression was not observed in uninfected corneal epithelium (not shown). Supplemental Movie 1 highlights the differential expression of tetherin in the epithelium by 3-dimensional confocal reconstructions of WT and STING$^{-/-}$ corneas. Punctate tetherin labeling in the deeper stromal layers of the corneas show infiltrating leukocytes which also express tetherin (Supplemental Movie 1).[29]

Tetherin expression was also evaluated in the TG by PCR at day 5 pi (Supplemental Figure 1b) in light of evidence showing tetherin expression in neurons[30,31] and the enhanced trafficking of HSV-1 from the cornea to the TG in STING$^{-/-}$ and CD118$^{-/-}$ mice observed herein (Supplemental Figure 1a). Though STING is required for tetherin expression in the corneal epithelium (Figure 4c, Supplemental Movie 1), tetherin is upregulated in the TG of STING$^{-/-}$ mice similarly to WT at an approximate 8-fold increase over UI yet conspicuously absent in CD118$^{-/-}$ TG at day 5 pi (Supplemental Figure 1b). The differential

induction of tetherin exemplifies the specificities and complexities of IFNα/β-mediated ISG stimulation in various tissues. Furthermore, it emphasizes that different anti-viral mechanisms control HSV-1 replication in different constituent cell types.

**Tetherin impedes local HSV-1 spread and neuroinvasion**

Lack of tetherin expression in the corneal epithelium of STING$^{-/-}$ and CD118$^{-/-}$ mice correlated with the observed increases in HSV-1 titers and unencumbered expression of HSV-1 antigen throughout the epithelium compared to WT animals. However, definitive evidence substantiating the role of tetherin in impeding local viral replication and neuroinvasion remained to be shown. siRNA transfection was used to limit tetherin expression in the corneas of WT mice pursuant to HSV-1 infection independent of ancillary IFNα/β-signaling deficiencies. Knockdown efficiency (Figure 5a) was greater than 70% at 48 hours pi at the transcript level, and trends in expression differences persisted at 72 hours pi. However, transcript expression differences were not statistically significant by the latter time point, therein demonstrating the transient nature of siRNA-mediated knockdown. Knockdown was validated at the protein level using confocal imaging to analyze the fluorescence intensity of tetherin immunolabeling in scramble and tetherin-specific siRNA-treated corneas at 72 hours pi (Figure 5b,c). Isotype control antibody labeling was used to validate the specificity of tetherin immunolabeling (Figure 5b).

Viral burden in the corneas and TG (Figure 5d) of siRNA-treated mice was subsequently measured. Local tetherin knockdown in the corneal epithelium led

to a significant increase in HSV-1 titer in the cornea and TG compared to scramble siRNA transfected controls at day 3 pi (Figure 5d). Consistent with the temporary effect of tetherin knockdown, no differences in viral titer were observed by day 5 pi in the cornea or TG (not shown) comparing the two siRNA-treated groups. Collectively, our data show that tetherin is indeed a functional viral restriction factor for HSV-1 *in vivo*. Specifically, we show that tetherin expression in the corneal epithelium is STING-dependent. Furthermore, we demonstrate that tetherin sequesters HSV-1 in the microenvironment of the corneal epithelium in order to inhibit local cell-cell spread, impede invasion of sensory nerve fibers, and consequentially restrict viral dissemination to the nervous system.

## DISCUSSION

Early IFNα/β induction through pathogen recognition receptor signaling is critical for the control of HSV-1 infection. Our previously reported data show that corneal viral titers in MyD88- or TRIF-deficient mice are no different than WT by day 5 pi;[8] however, the corneal HSV-1 titer at day 5 pi in STING$^{-/-}$ mice was more consistent with the highly susceptible CD118$^{-/-}$ mice in the present study. Collectively, our data demonstrate that a TLR-independent, STING-dependent process mediates initial and sustained resistance to acute HSV-1 infection in the cornea prior to the induction of an adaptive immune response.

The basic resident cell composition of the murine cornea includes epithelial cells, stromal keratocytes, and endothelial cell layers in addition to

tissue-resident leukocytes, sensory nerve fibers and peripheral vasculature. Each of these cell types and structures likely provide distinct contributions to defense against HSV-1 infection that collectively combat viral replication and spread. Likewise, corneal HSV-1 infection may directly or indirectly elicit unique pathologies affecting each of these components. Blood and lymphatic vessels surrounding the cornea play unique roles during infection by facilitating leukocyte influx and efflux of extracellular fluid and macromolecules, respectively.

Stark differences were observed with respect to corneal pathology comparing STING$^{-/-}$ to CD118$^{-/-}$ mice despite a similar viral burden. The severe corneal edema exhibited by CD118$^{-/-}$ mice correlated with a hyperacute sensory deficit following HSV-1 infection. These findings support established notions that inflammatory processes in the cornea induce loss of innervation, and that local trophic factors maintain or restore the delicate corneal sensory fibers following injury or pathogenic insult.[21,32,33] The present investigation expands the mechanistic understanding of corneal denervation following HSV-1 infection by identifying sensation loss transpires independent of the viral burden locally in the cornea or in the TG.

Corneal HSV-1 infection with high-titer inoculums can elicit inflammatory neovascularization during the acute stage of infection.[34] Moreover, lymphatic vessels are infected and destroyed by HSV-1 absence of IFNα/β signaling.[26] Observations from the present investigation suggest that while STING is critical for containment of HSV-1 replication and spread in the corneal epithelium, an auxiliary STING-independent yet IFNα/β-dependent pathway protects the corneal

stroma and peripheral lymphatic vessels from HSV-1 infection and resultant edema.

The selective loss of mast cells in CD118$^{-/-}$ but not in STING$^{-/-}$ mice again supports the importance of STING-independent IFNα/β-signaling pathways in the maintenance of the corneal architecture. Mast cells likely provide support for peri-corneal lymphatic vessels and may also contribute to inflammatory lymphangiogenesis in the cornea as has been shown in other sites.[35–37] Our findings collectively emphasize the importance of IFNα/β-signaling not only with respect to its anti-viral properties, but highlight its role in maintaining tissue integrity and preservation of visual acuity.

Multiple studies have established that IFNα/β signaling in both resident and bone marrow-derived cells is critical for resistance to acute HSV-1 infection in the cornea.[23,26] We observed a profound increase in the myeloid cell infiltrate in corneas of STING$^{-/-}$ mice relative to WT consistent with a recent report describing the role of STING-dependent suppression of excessive immune activation.[38] Our lab has previously shown that of the infiltrating myeloid-lineage leukocytes, inflammatory monocytes (CD45$^{+}$ Gr-1$^{+}$ F4/80$^{+}$) facilitate virus clearance and are recruited by CCL2 following acute HSV-1 infection in the cornea.[23]

We have now identified two distinct monocyte populations in the cornea at day 5 pi. Of these, the Ly6C$^{+}$ Ly6G$^{low}$ population reflects protective inflammatory monocytes. The secondary Ly6C$^{+}$ Ly6G$^{high}$ monocyte population observed in the cornea has been described in hypoxic metastatic niches[39–41] and during

pulmonary viral infection concomitant with a lack of IFNα/β signaling and altered chemokine production.[42] The concept of distinct monocyte subsets with notable plasticity, phenotypic variation, and functional diversity is now well established for a wide variety of pathologies.[43–47]

Inflammatory monocytes are efficiently recruited to the corneas of STING$^{-/-}$ mice and prevent excessive tissue pathology beyond the surface barrier epithelium. *In vitro* data indicate that human macrophages and murine myeloid dendritic cells utilize a STING-dependent pathway for recognition of HSV-1 and subsequent induction of IFNβ, cytokine production, and autophagy.[48–50] Accordingly, we investigated MHC II upregulation as an indicator of monocyte activation in the absence of STING, and found no defect compared to WT monocytes in vitro, though a defect in MHC II upregulation was observed in STING$^{-/-}$ macrophages (Supplemental Figure 2c,d).

Anti-viral restriction factors serve as wardens for controlling viral infections by arresting virus replication and spread. Tetherin is a type II transmembrane protein that shares topographical homology with several prion proteins which express multiple membrane anchors, including a glycosyl-phosphatidylinositol (GPI) anchor.[20] Tetherin is upregulated by IFN signaling (IFN-α/β, -γ, and -λ) and is inducible in polarized epithelial cells, constitutively expressed by blood vessel endothelial cells and many leukocytes.[18,29,51] Tetherin promotes endocytosis and degradation of enveloped virions bound to the cell surface, and is implicated in transcription of NFκB-regulated cytokines.[52]

Following successful replication of HSV-1 in epithelial cell nuclei, nascent HSV-1 virions must egress through the nuclear membrane, *trans*-Golgi network, and plasma membrane to infect neighboring cells.[53] The GPI anchor of tetherin facilitates attachment to and retention of enveloped viruses upon virion budding from the trans-Golgi network and plasma membranes to reduce cell-cell spread.[54] Furthermore, reports indicate that HSV-1 employs at least two distinct mechanisms to counteract tetherin and evade restriction *in vitro*.[55,56] However, the *in vivo* relevance of tetherin with respect to HSV-1 infection has not been reported. Our *in vivo* data show that tetherin sequesters HSV-1 replication and spread in the cornea in addition to restricting neuroinvasion and dissemination of the virus to peripheral nerve ganglia. Furthermore, our findings detail a novel mechanism of HSV-1 restriction involving a STING-dependent, IFNα/β-mediated signaling pathway that induces tetherin expression in epithelial cells within the ocular mucosae.

## METHODS

**Mice and virus.** C57BL/6J WT and STING$^{-/-}$ mice were obtained from the Jackson Laboratory. CD118$^{-/-}$ and STING$^{-/-}$ mice were bred in-house. All mice were maintained in a specific pathogen-free vivarium at the Dean McGee Eye Institute (University of Oklahoma Health Sciences Center, Oklahoma City, OK). Mice were euthanized by cardiac perfusion with 10-15 ml of 1x PBS. All experimental procedures were conducted in accordance with protocols approved by Institutional Animal Care and Use Committees. HSV-1 strain McKrae was used for all experiments; the stock concentration was 7.07x10$^{7}$ plaque forming units (pfu) per ml.

**Infection and plaque assays.** Six to twelve week old mice were anesthetized by ketamine (100 mg/kg) and xylazine (6.6 mg/kg) injection *ip*. Following partial epithelial debridement of the cornea using a 25-gauge needle, an inoculum of 1000 pfu of HSV-1 was applied to each eye. Tissues collected from euthanized animals for standard plaque assays were homogenized and supernatants titered on confluent CCL-81 Vero cell (ATCC, Manassas, VA) monolayers in microtiter plates as described previously.[28]

**Corneal pathology.** Ultrasound pachymetry was utilized to monitor corneal thickness and edema following infection using a Corneo-Gage Plus digital pachymeter (Sonogage, Cleveland OH) as described previously.[28] Corneal sensation or blink reflex sensitivity was evaluated using a handheld Cochet-Bonnet esthesiometer as described previously.[21] Cochet-Bonnet filament length-

418 scores were interpolated into threshold sensitivity pressures using conversions
419 provided by the manufacturer.
420 **Gene array.** Transcript expression studies on corneas were performed using
421 PrimePCR pathway analysis technology from Bio-Rad (Hercules, CA) for
422 selected genes according to the manufacturer's directions. RNA was isolated
423 from corneas and converted into cDNA as described previously.[8] Relative gene
424 expression was calculated by the standard $2^{-\Delta\Delta Ct}$ method using *GAPDH* and *TBP*
425 as reference genes following semi-quantitative real time PCR using a CFX
426 Connect thermocycler and PrimePCR technology (Bio-Rad). Transcripts
427 evaluated are listed in Figure 2. Gene expression profiles represented by the
428 cluster image map in Figure 2 were generated using the National Cancer
429 Institute's CIMminer tool freely accessible online.
430 **Flow cytometry.** Corneas were harvested from enucleated eyes of euthanized
431 animals and digested in 2 mg/ml type 1 collagenase from *Clostridium*
432 *histolyticum* (Sigma-Aldrich, St. Louis, MO) in RPMI 1640 media supplemented
433 with 10% FBS, gentamicin, and antibiotic/antimycotic cocktail (Invitrogen, Grand
434 Island, NY) for 2-2.5 hours at 37°C with gentle mechanical trituration every 15
435 minutes. The suspension was subsequently filtered through 40µm mesh,
436 washed with 1% BSA in 1x PBS (wash buffer), pelleted, and labeled for flow
437 cytometric analysis. Cells were immunolabeled for 30 minutes at 4°C following a
438 15 minute incubation with anti-CD16/32 Fc block. Antibodies were obtained from
439 AbD Serotec (Raleigh, NC), eBioscience (San Diego, CA), BD Biosciences (San
440 Jose, CA) to label CD11b, CD45, F4/80, I-A/I-E, Ly6C, and Ly6G leukocyte

antigens. Following labeling, cells were washed twice, fixed in 1% PFA (Sigma-Aldrich) and stored overnight at 4°C. Samples were pelleted and resuspended in 1 ml wash buffer for analysis on a MacsQuant flow cytometer (Miltenyi Biotech, Bergisch Gladbach, Germany).

**Immunoassays.** Corneas harvested at the indicated times pi and homogenized in 1x PBS containing 1x protease inhibitor set 1 (EMD Millipore, Billerica, MA). Supernatants were used at the indicated times pi to evaluate protein concentrations of IFNα by ELISA (eBioscience) or CCL2, CCL20, IFNγ, IL-1β, and IL-17 by Bio-Plex (Biorad) suspension array according to the manufacturers' directions.

**Splenocyte isolation and cultures.** Spleens were harvested from euthanized mice, teased into single cell suspensions, and depleted of erythrocytes as described previously.[28] Immunomagnetic beads (Miltenyi Biotech) were used to isolate $CD11b^+$ splenocytes by positive selection according to the manufacturer's instructions. Cultures of $1x10^5$ cells were incubated at 37˚C for 24-48 hours at 5% $CO_2$ in 1 ml RPMI 1640 media supplemented with 10% FBS, gentamicin, and antibiotic/antimycotic cocktail (Invitrogen). Supernatants were collected for plaque assay and cells were labeled for analysis by flow cytometry.

**Microscopy.** For confocal microscopic analysis of vasculature, mast cells, and tetherin expression, corneolimbal buttons were harvested from enucleated eyes of euthanized animals, fixed in 4% PFA for 30 minutes at 4°C, washed 3 times for 15 minutes in 1% Triton X-100 (Sigma-Aldrich) in 1x PBS, and immunolabeled or stained. Samples were washed between primary and

secondary antibodies. Antibodies used to label cornea whole mounts were obtained from Abcam (Cambridge, MA), eBioscience, Dako (Carpinteria, CA), EMD Millipore, or Jackson ImmunoResearch (WestGrove, PA). FITC-conjugated avidin was used to stain peri-corneal mast cells (Biolegend, San Diego, CA) as shown previously.[28] Flat mounts of the tissue were prepared and imaged using an Olympus FV500 confocal microscope (Center Valley, PA). Olympus Fluoview and iMovie (Apple, Cupertino, CA) software were used to generate 3D Z-stack renderings and video highlighting the topographical localization of tetherin expression in the cornea (Supplemental Movie 1).

***In vivo* transfection.** Ambion Silencer Select siRNA (Invitrogen) was used for corneal knockdown experiments and transfection mediated using lipofectamine 2000 (Invitrogen) as described previously.[8] Briefly, partial epithelial debridement of corneas of anesthetized WT mice was conducted to prepare the eye for transfection. Next, 3.33 µmol tetherin-specific or nonspecific scramble control siRNA in supplement-free DMEM media was applied to each cornea in a 10 µl eye drop containing 5 µl Lipofecamine 2000 (Invitrogen). siRNA sequences were designed and validated by the manufacturer. Mice were infected with HSV-1 16 hours post-transfection. On days 2, 3, or 5 pi, corneas were harvested for plaque assay and validation of knockdown efficiency. Tetherin transcript expression was quantified using PrimePCR technology (Biorad) as described for the gene array. Tetherin protein was imaged in immunolabeled cornea flat mounts by confocal microscopy.

**Statistical analysis.** Normal distribution of all data was assumed *a priori*. Graphical representations of data reflect mean ± SEM. Statistical analysis of all data was performed using GraphPad Prism 5 (La Jolla, CA). One-and two-way ANOVAs were used to distinguish differences among data sets while significance thresholds for sample means were identified using Student-Newman-Keuls multiple comparison tests or Bonferroni posttests, respectively. A standard unpaired Student's T test was used when applicable.

**Online supplemental material.** Supplementary data is available online at www.nature.com/mi


## ACKNOWLEDGEMENTS

This work was supported by National Institutes of Health / National Eye Institute Grants R01 EY021238, P30 EY021725, and T32 EY023202. Additional support was provided by an unrestricted grant from Research to Prevent Blindness. The content of this manuscript is solely the responsibility of the authors and does not necessarily represent the official views of the NIH. The authors would like to thank Mark Dittmar and the DMEI Vivarium staff for their help in maintaining our animals; Helen Rosenberg, Ph.D. for the original source of $CD118^{-/-}$ mice; and Meghan Carr, Jeremy Jinkins, and Min Zheng for technical assistance. The authors have no commercial or financial conflicts of interest.

## REFERENCES


1. Perry, A. K., Chen, G., Zheng, D., Tang, H. & Cheng, G. The host type I interferon response to viral and bacterial infections. *Cell Res.* **15,** 407–422 (2005).
2. Ivashkiv, L. B. & Donlin, L. T. Regulation of type I interferon responses. *Nat. Rev. Immunol.* **14,** 36–49 (2013).
3. Randall, R. E. & Goodbourn, S. Interferons and viruses: an interplay between induction, signalling, antiviral responses and virus countermeasures. *J. Gen. Virol.* **89,** 1–47 (2008).
4. Duggal, N. K. & Emerman, M. Evolutionary conflicts between viruses and restriction factors shape immunity. *Nat. Rev. Immunol.* **12,** 687–695 (2012).
5. Barber, G. N. Innate immune DNA sensing pathways: STING, AIMII and the regulation of interferon production and inflammatory responses. *Curr. Opin. Immunol.* **23,** 10–20 (2011).
6. Rathinam, V. A. K. & Fitzgerald, K. A. Innate immune sensing of DNA viruses. *Virology* **411,** 153–162 (2011).
7. Wu, J. & Chen, Z. J. Innate Immune Sensing and Signaling of Cytosolic Nucleic Acids. *Annu. Rev. Immunol.* **32,** 461–488 (2014).
8. Conrady, C. D., Zheng, M., Fitzgerald, K. A., Liu, C. & Carr, D. J. J. Resistance to HSV-1 infection in the epithelium resides with the novel innate sensor, IFI-16. *Mucosal Immunol.* **5,** 173–183 (2012).
9. Burdette, D. L. & Vance, R. E. STING and the innate immune response to nucleic acids in the cytosol. *Nat. Immunol.* **14,** 19–26 (2013).

529 10. Tanaka, Y. & Chen, Z. J. STING specifies IRF3 phosphorylation by TBK1 in the
530 cytosolic DNA signaling pathway. *Sci. Signal.* **5,** ra20 (2012).
531 11. Unterholzner, L. *et al.* IFI16 is an innate immune sensor for intracellular DNA.
532 *Nat. Immunol.* **11,** 997–1004 (2010).
533 12. Orzalli, M. H., DeLuca, N. A. & Knipe, D. M. PNAS Plus: Nuclear IFI16 induction of
534 IRF-3 signaling during herpesviral infection and degradation of IFI16 by the
535 viral ICP0 protein. *Proc. Natl. Acad. Sci.* **109,** E3008–E3017 (2012).
536 13. Lin, R., Noyce, R. S., Collins, S. E., Everett, R. D. & Mossman, K. L. The herpes
537 simplex virus ICP0 RING finger domain inhibits IRF3- and IRF7-mediated
538 activation of interferon-stimulated genes. *J. Virol.* **78,** 1675–1684 (2004).
539 14. Paladino, P., Collins, S. E. & Mossman, K. L. Cellular Localization of the Herpes
540 Simplex Virus ICP0 Protein Dictates Its Ability to Block IRF3-Mediated Innate
541 Immune Responses. *PLoS ONE* **5,** e10428 (2010).
542 15. Royer, D. J., Cohen, A. W. & Carr, D. J. The current state of vaccine development
543 for ocular HSV-1 infection. *Expert Rev. Ophthalmol.* **10,** 113–126 (2015).
544 16. Conrady, C. D. *et al.* Microglia and a Functional Type I IFN Pathway Are Required
545 To Counter HSV-1–Driven Brain Lateral Ventricle Enlargement and Encephalitis.
546 *J. Immunol.* **190,** 2807–2817 (2013).
547 17. Bonini, S., Rama, P., Olzi, D. & Lambiase, A. Neurotrophic keratitis. *Eye* **17,** 989–
548 995 (2003).
549 18. Hotter, D., Sauter, D. & Kirchhoff, F. Emerging role of the host restriction factor
550 tetherin in viral immune sensing. *J. Mol. Biol.* **425,** 4956–4964 (2013).

19. Li, S. X. *et al.* Tetherin promotes the innate and adaptive cell-mediated immune response against retrovirus infection in vivo. *J. Immunol. Baltim. Md 1950* **193,** 306–316 (2014).
20. Sauter, D. Counteraction of the multifunctional restriction factor tetherin. *Front. Microbiol.* **5,** (2014).
21. Chucair-Elliott, A. J., Zheng, M. & Carr, D. J. J. Degeneration and regeneration of corneal nerves in response to HSV-1 infection. *Invest. Ophthalmol. Vis. Sci.* **56,** 1097–1107 (2015).
22. Testoni, B. *et al.* Chromatin dynamics of gene activation and repression in response to interferon alpha (IFNα) reveal new roles for phosphorylated and unphosphorylated forms of the transcription factor STAT2. *J. Biol. Chem.* **286,** 20217–20227 (2011).
23. Conrady, C. D., Zheng, M., Mandal, N. A., van Rooijen, N. & Carr, D. J. J. IFN-α-driven CCL2 production recruits inflammatory monocytes to infection site in mice. *Mucosal Immunol.* **6,** 45–55 (2013).
24. Shi, C. & Pamer, E. G. Monocyte recruitment during infection and inflammation. *Nat. Rev. Immunol.* **11,** 762–774 (2011).
25. Ishikawa, H., Ma, Z. & Barber, G. N. STING regulates intracellular DNA-mediated, type I interferon-dependent innate immunity. *Nature* **461,** 788–792 (2009).
26. Bryant-Hudson, K. M. *et al.* HSV-1 targets lymphatic vessels in the eye and draining lymph node of mice leading to edema in the absence of a functional type I interferon response. *Am. J. Pathol.* **183,** 1233–1242 (2013).

27. Wernersson, S. & Pejler, G. Mast cell secretory granules: armed for battle. *Nat. Rev. Immunol.* **14,** 478–494 (2014).

28. Royer, D. J., Zheng, M., Conrady, C. D. & Carr, D. J. J. Granulocytes in Ocular HSV-1 Infection: Opposing Roles of Mast Cells and Neutrophils. *Invest. Ophthalmol. Vis. Sci.* **56,** 3763–3775 (2015).

29. Erikson, E. *et al.* In vivo expression profile of the antiviral restriction factor and tumor-targeting antigen CD317/BST-2/HM1.24/tetherin in humans. *Proc. Natl. Acad. Sci. U. S. A.* **108,** 13688–13693 (2011).

30. Sarojini, S., Theofanis, T. & Reiss, C. S. Interferon-induced tetherin restricts vesicular stomatitis virus release in neurons. *DNA Cell Biol.* **30,** 965–974 (2011).

31. Holmgren, A. M., Miller, K. D., Cavanaugh, S. E. & Rall, G. F. Bone marrow stromal antigen-2 (Bst2)/tetherin is induced in neurons by type I interferon and viral infection, but is dispensable for protection against neurotropic viral challenge. *J. Virol.* JVI.01745–15 (2015). doi:10.1128/JVI.01745-15

32. Sarkar, J. *et al.* CD11b+GR1+ myeloid cells secrete NGF and promote trigeminal ganglion neurite growth: implications for corneal nerve regeneration. *Invest. Ophthalmol. Vis. Sci.* **54,** 5920–5936 (2013).

33. Guaiquil, V. H. *et al.* VEGF-B selectively regenerates injured peripheral neurons and restores sensory and trophic functions. *Proc. Natl. Acad. Sci. U. S. A.* **111,** 17272–17277 (2014).

34. Wuest, T. R. & Carr, D. J. J. VEGF-A expression by HSV-1-infected cells drives corneal lymphangiogenesis. *J. Exp. Med.* **207,** 101–115 (2010).

35. Kunder, C. A., St John, A. L. & Abraham, S. N. Mast cell modulation of the vascular and lymphatic endothelium. *Blood* **118,** 5383–5393 (2011).
36. Raica, M. *et al.* Mast cells stimulate lymphangiogenesis in the gingiva of patients with periodontal disease. *Vivo Athens Greece* **29,** 29–34 (2015).
37. Marone, G., Varricchi, G., Loffredo, S. & Granata, F. Mast cells and basophils in inflammatory and tumor angiogenesis and lymphangiogenesis. *Eur. J. Pharmacol.* (2015). doi:10.1016/j.ejphar.2015.03.088
38. Sharma, S. *et al.* Suppression of systemic autoimmunity by the innate immune adaptor STING. *Proc. Natl. Acad. Sci. U. S. A.* **112,** E710–717 (2015).
39. Kowanetz, M. *et al.* Granulocyte-colony stimulating factor promotes lung metastasis through mobilization of Ly6G+Ly6C+ granulocytes. *Proc. Natl. Acad. Sci. U. S. A.* **107,** 21248–21255 (2010).
40. Yang, X. D. *et al.* Histamine deficiency promotes inflammation-associated carcinogenesis through reduced myeloid maturation and accumulation of CD11b+Ly6G+ immature myeloid cells. *Nat. Med.* **17,** 87–95 (2011).
41. Sceneay, J. *et al.* Primary tumor hypoxia recruits CD11b+/Ly6Cmed/Ly6G+ immune suppressor cells and compromises NK cell cytotoxicity in the premetastatic niche. *Cancer Res.* **72,** 3906–3911 (2012).
42. Seo, S.-U. *et al.* Type I interferon signaling regulates Ly6C(hi) monocytes and neutrophils during acute viral pneumonia in mice. *PLoS Pathog.* **7,** e1001304 (2011).
43. Gordon, S. & Taylor, P. R. Monocyte and macrophage heterogeneity. *Nat. Rev. Immunol.* **5,** 953–964 (2005).

618 44. Strauss-Ayali, D., Conrad, S. M. & Mosser, D. M. Monocyte subpopulations and
619 their differentiation patterns during infection. *J. Leukoc. Biol.* **82,** 244–252
620 (2007).
621 45. Rose, S., Misharin, A. & Perlman, H. A novel Ly6C/Ly6G-based strategy to analyze
622 the mouse splenic myeloid compartment. *Cytom. Part J. Int. Soc. Anal. Cytol.* **81,**
623 343–350 (2012).
624 46. Mitchell, A. J., Roediger, B. & Weninger, W. Monocyte homeostasis and the
625 plasticity of inflammatory monocytes. *Cell. Immunol.* **291,** 22–31 (2014).
626 47. Xiong, H. & Pamer, E. G. Monocytes and infection: modulator, messenger and
627 effector. *Immunobiology* **220,** 210–214 (2015).
628 48. Zhang, Z. *et al.* The helicase DDX41 senses intracellular DNA mediated by the
629 adaptor STING in dendritic cells. *Nat. Immunol.* **12,** 959–965 (2011).
630 49. Rasmussen, S. B. *et al.* Activation of autophagy by α-herpesviruses in myeloid
631 cells is mediated by cytoplasmic viral DNA through a mechanism dependent on
632 stimulator of IFN genes. *J. Immunol.* **187,** 5268–5276 (2011).
633 50. Horan, K. A. *et al.* Proteasomal degradation of herpes simplex virus capsids in
634 macrophages releases DNA to the cytosol for recognition by DNA sensors. *J.*
635 *Immunol.* **190,** 2311–2319 (2013).
636 51. Rollason, R., Korolchuk, V., Hamilton, C., Jepson, M. & Banting, G. A
637 CD317/tetherin-RICH2 complex plays a critical role in the organization of the
638 subapical actin cytoskeleton in polarized epithelial cells. *J. Cell Biol.* **184,** 721–
639 736 (2009).

52. Galão, R. P., Le Tortorec, A., Pickering, S., Kueck, T. & Neil, S. J. D. Innate Sensing of HIV-1 Assembly by Tetherin Induces NFκB-Dependent Proinflammatory Responses. *Cell Host Microbe* **12,** 633–644 (2012).

53. Johnson, D. C., Wisner, T. W. & Wright, C. C. Herpes Simplex Virus Glycoproteins gB and gD Function in a Redundant Fashion To Promote Secondary Envelopment. *J. Virol.* **85,** 4910–4926 (2011).

54. Martin-Serrano, J. & Neil, S. J. D. Host factors involved in retroviral budding and release. *Nat. Rev. Microbiol.* **9,** 519–531 (2011).

55. Zenner, H. L., Mauricio, R., Banting, G. & Crump, C. M. Herpes simplex virus 1 counteracts tetherin restriction via its virion host shutoff activity. *J. Virol.* **87,** 13115–13123 (2013).

56. Blondeau, C. *et al.* Tetherin restricts herpes simplex virus 1 and is antagonized by glycoprotein M. *J. Virol.* **87,** 13124–13133 (2013).

## FIGURE LEGENDS

**Figure 1: Viral burden and acute pathology in the cornea.** (a) Viral titers at day 5 pi in fellow corneas of WT, STING$^{-/-}$, and CD118$^{-/-}$ mice (*n* = 7-8 mice/group, 3 independent experiments). (b) Corneal sensitivity measured using a Cochet-Bonnet esthesiometer on day 5 pi. Black bars reflect Cochet-Bonnet score/ filament length in cm (left axis); red open circles reflect corneal sensation threshold in g/mm$^2$ (right axis), *i.e.* minimum pressure required to elicit a blink response (*n* = 16 corneas/group, 3 independent experiments). (c) Ultrasound pachymetry measurements of corneal thickness in uninfected and infected mice through day 5 pi (*n* = 14-20 corneas/group/time point; 4 independent experiments). For panel c, * indicates differences between WT and STING$^{-/-}$ or CD118$^{-/-}$; ^ indicates differences between STING$^{-/-}$ and CD118$^{-/-}$ mice; significance threshold: *$p < 0.05$, **$p < 0.01$, ***$p < 0.001$. (d) Representative 10x confocal images illustrating localization of viral antigen in cornea whole mounts at day 5 pi; scale bar = 100 μm. (e) 60x images of viral lesions from (d) with 60 μm z-stack focal projections illustrating HSV-1 labeling in the epithelium and penetration into the stroma; scale bar = 20 μm.

**Figure 2: IFNα/β regulated gene expression.** (a) Cluster image map summary of selected IFNα/β-regulated transcript expression relative to the geometric mean of GAPDH and TBP expression at day 5 pi (standardized to UI WT corneas using the $2^{-\Delta\Delta CT}$ method). (b) Quantified expression values for selected genes (*n* = 6-8 mice/group; 3 independent experiments). For panel b, * indicates differences

678 between WT and STING$^{-/-}$ or CD118$^{-/-}$; ^ indicates differences between STING$^{-/-}$
679 and CD118$^{-/-}$ mice; *$p$ < 0.05, **$p$ < 0.01, ***$p$ < 0.001. Bst2 (Bone marrow
680 stromal antigen 2; tetherin), Ch25h (cholesterol 25 hydroxylase), Eif2ak2
681 (eukaryotic initiation factor 2α kinase 2), Ifnb (IFNβ), Irf (IFN regulatory factor),
682 Nos2 (inducible nitric oxide synthase), Oas (oligoadenylate synthetase), Rnasel
683 (2'-5' Oas-dependent ribonuclease), Wars (tryptophan aminoacyl-tRNA
684 synthetase).
685
686 **Figure 3: Leukocyte recruitment and function.** Total cornea-infiltrating CD45+
687 CD11b+ myeloid-lineage leukocytes (a), Ly6C$^{low}$ Ly6G$^{hi}$ PMN (b), Ly6C$^{+}$ Ly6G$^{high}$
688 monocytes (c), Ly6C$^{+}$ Ly6G$^{low}$ monocytes (d) at day 5 pi ($n$ = 8 mice/group; 3
689 independent experiments). (e) Ratio of cornea-infiltrating Ly6G$^{high}$:Ly6G$^{low}$ Ly6C$^{+}$
690 monocytes. (f) Representative flow plots of cornea-infiltrating CD45+ CD11b+
691 myeloid-lineage leukocyte subsets in WT, STING$^{-/-}$ and CD118$^{-/-}$ mice are
692 featured in the following gates: Ly6C$^{+}$ Ly6G$^{low}$ monocytes (top central), Ly6C$^{+}$
693 Ly6G$^{hi}$ monocytes (top right), Ly6C$^{low}$ Ly6G$^{hi}$ PMN (lower right). Protein
694 concentrations of IFNα$_{2,4}$ and IFNγ (g); monocyte-chemotactic cytokines CCL2
695 (c-c motif chemokine ligand 2) and CCL20 (h); and inflammatory mediators IL-1β
696 and IL-17 (i) in cornea pairs at day 5 pi ($n$ = 10-17 mice/group infected, 1-3 UI
697 controls; 2-3 independent experiments). For panels (g - i), * indicates differences
698 between WT and STING$^{-/-}$ or CD118$^{-/-}$; ^ indicates differences between STING$^{-/-}$
699 and CD118$^{-/-}$ mice. (j) Viral titers from supernatants of CD11b-enriched
700 splenocytes cultured *in vitro* with HSV-1 for 48 hours at various multiplicities of

infection (MOI) (*n* = 3-6 culture samples per group; 2 independent experiments). Significance thresholds: *$p < 0.05$, **$p < 0.01$, ***$p < 0.001$ comparing the indicated groups.

**Figure 4: Vasculature, mast cells, and tetherin expression at day 5 pi.** Representative 10x immunofluorescent confocal images of cornea flat mounts prepared at day 5 pi from 3-5 mice/group are shown. Lymphatic and blood vessels were labeled using Lyve-1 and CD31-specific antibodies, respectively (a). Mast cells stained with FITC-avidin reside along the limbal margin demarcated by Lyve-1 positive lymphatic vessels (b). Tetherin immunolabeling (c) highlights the constitutive tetherin expression on blood but not lymphatic vessels, and IFN-inducible expression in the epithelium (images in panels a and c are of the same sample). White dotted lines demarcate the separation between the cornea and limbus. Scale bars = 100 μm.

**Figure 5: Tetherin restricts local HSV-1 spread and neuroinvasion *in vivo*.** Corneas of WT mice were transfected with scramble or tetherin-specific siRNA, infected, animals euthanized at day 3 or 5 pi, corneas and TG harvested for PCR, 40x confocal imaging, or plaque assay on corneas and TG. (a) Quantification of tetherin expression relative to GAPDH and TBP expression in transfected corneas at 48 and 72 hours pi (*n* = 5 animals/group/end point; 2 independent experiments; * = *p* value ≤ 0.05). (b) Representative images of isotype or tetherin-specific antibody labeling with DAPI stain for contrast in the

724 corneal epithelial layers of target or scramble siRNA transfected corneas at day 3
725 pi (scale bar = 20 μm). (c) Relative siRNA-mediated tetherin protein knockdown
726 shown as images and isometric histogram projections of tetherin MFI from panel
727 b. Imaging was conducted on 3-4 corneas/group; 2-3 independent experiments.
728 (d) HSV-1 titers in individual scramble control and tetherin-specific siRNA
729 transfected mouse corneas (representative data from 1 of 2 experiments shown;
730 n = 6-7 corneas/group total) and TG (*n* = 8-9 TG/group; 3 independent
731 experiments); * = $p < 0.05$ comparing scramble siRNA to tetherin siRNA
732 transfected groups.

## DESCRIPTIONS FOR SUPPLEMENTAL MATERIAL

**Supplemental Figure 1.** (a) HSV-1 titers at day 3 pi (*n* = 6 TG per group; 2 independent experiments) . (b) Relative expression of tetherin in the TG at day 5 pi (*n* = 8-12 TG/group; 3 independent experiments). For panels (a,b), * indicates differences between WT and STING$^{-/-}$ or CD118$^{-/-}$; ^ indicates differences between STING$^{-/-}$ and CD118$^{-/-}$ mice. Significance thresholds: *$p < 0.05$, ***$p < 0.001$ comparing the indicated groups.

**Supplemental Figure 2.** (a) HSV-1 titers in splenocyte culture supernatants at 24 hours pi (b) Representative flow plots of splenocytes freshly isolated from UI WT or STING$^{-/-}$ mice pregated on CD45+ CD11b$^{+}$ to show equal heterogeneity of the myeloid cell subsets based on Ly6C and F4/80 antigen expression. (c) Representative flow plots for uninfected CD11b$^{+}$ splenocyte cultures pregated on CD45$^{+}$ cells at 24 hours pi. Macrophages (F4/80$^{+}$ Ly6C$^{–}$) are gated in black boxes and monocyes (Ly6C$^{mid/high}$ F4/80$^{high/mid}$) in blue and pink ovals, respectively. Histograms show MHC II expression from each gated population. (d) Cultured CD11b$^{+}$ splenocytes inoculated at MOI = 10 and analyzed as in (c). (d) Isotype antibody labeling of MHC II in WT HSV-1 inoculated (MOI = 10) CD11b$^{+}$ cultures at 24 hours pi. All experiments: *n* = 3-6 culture samples per group; 2 independent experiments.

**Supplemental Movie 1.** Localization of tetherin expression in a 3-dimensional reconstruction of a confocal full-thickness Z-stack image of WT and STING$^{-/-}$ corneas captured at 60x magnification on day 3 pi. A honeycomb-like patterning is observed in the corneal epithelium, but labeling is punctate in the deeper stromal layer consistent with tetherin expression on infiltrating leukocytes.

# Figure 1

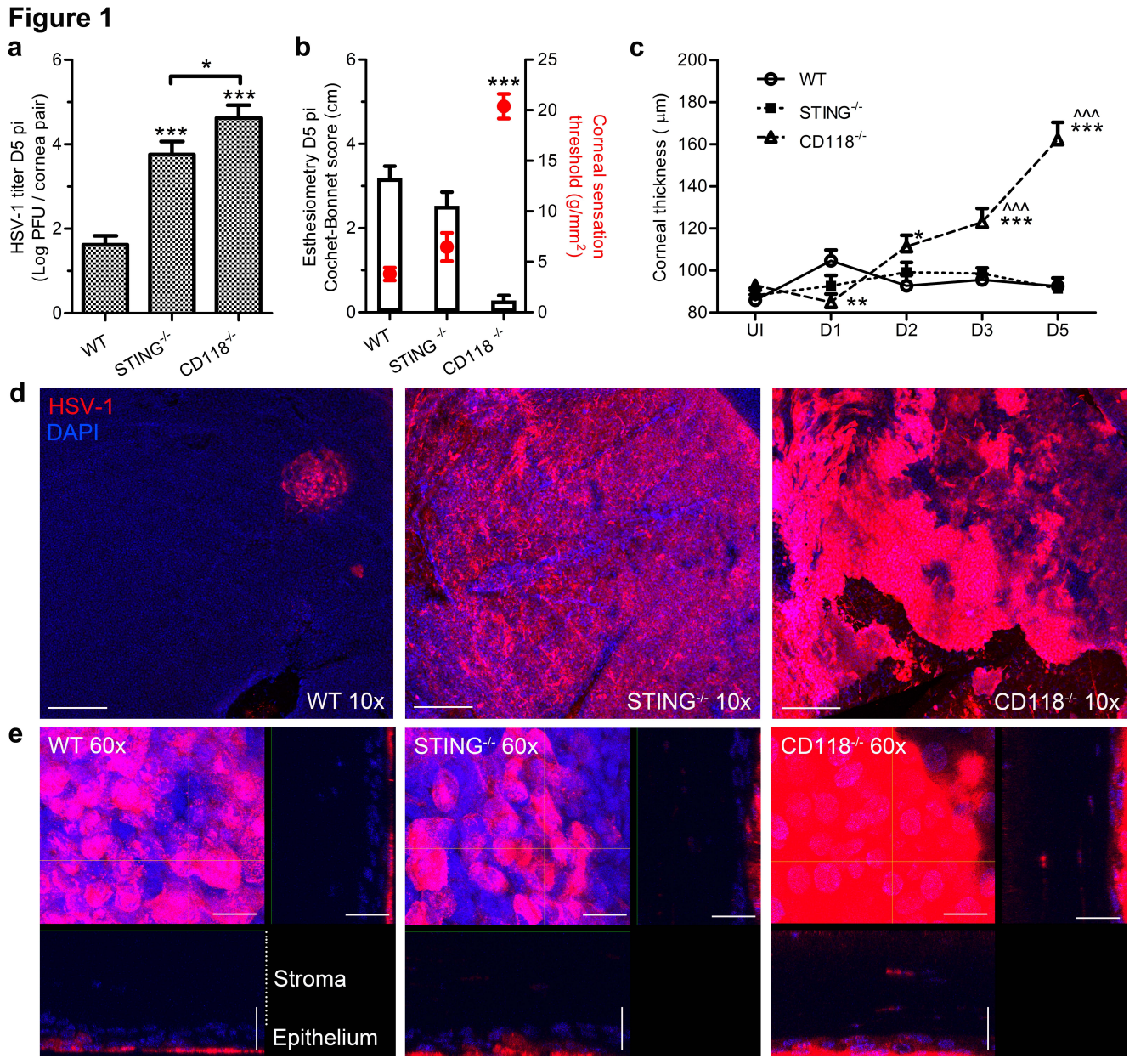
a
HSV-1 titer D5 pi
(Log PFU / cornea pair)
6
4
2
0
*
***
***
WT
STING-/-
CD118-/-
b
Esthesiometry D5 pi
Cochet-Bonnet score (cm)
Corneal sensation
threshold (g/mm2)
25
20
15
10
5
***
c
Corneal thickness ( µm)
200
180
160
140
120
100
80
WT
STING-/-
CD118-/-
^^^
***
UI
D1
D2
D3
D5
d
HSV-1
DAPI
WT 10x
STING-/- 10x
CD118-/- 10x
e
WT 60x
STING-/- 60x
CD118-/- 60x
Stroma
Epithelium

# Figure 2

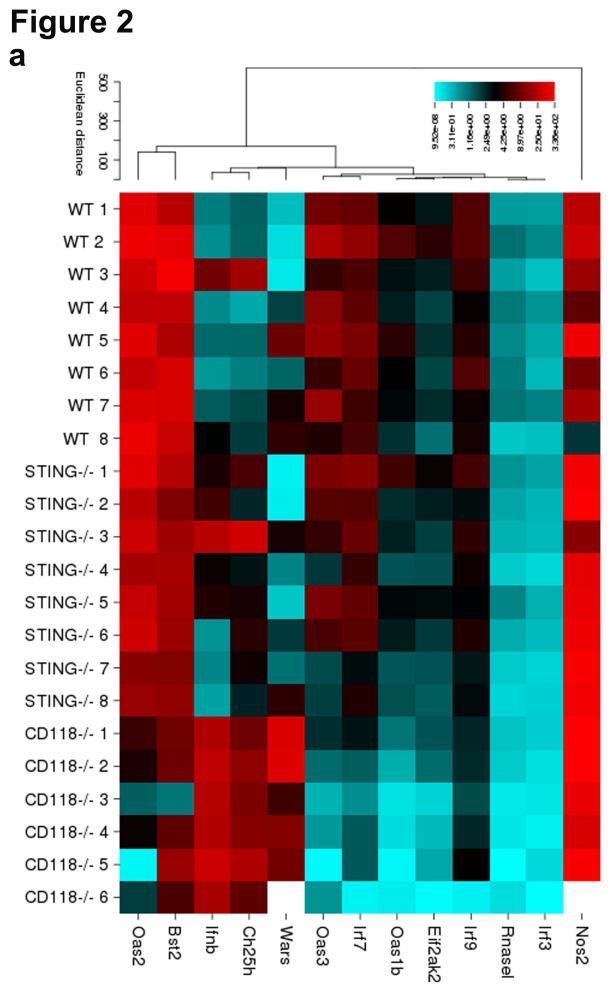
a
Euclidean distance
500
300
100
WT 1
WT 2
WT 3
WT 4
WT 5
WT 6
WT 7
WT 8
STING-/- 1
STING-/- 2
STING-/- 3
STING-/- 4
STING-/- 5
STING-/- 6
STING-/- 7
STING-/- 8
CD118-/- 1
CD118-/- 2
CD118-/- 3
CD118-/- 4
CD118-/- 5
CD118-/- 6
Oas2
Bst2
Ifnb
Ch25h
Wars
Oas3
Irf7
Oas1b
Eif2ak2
Irf9
Rnasel
Irf3
Nos2

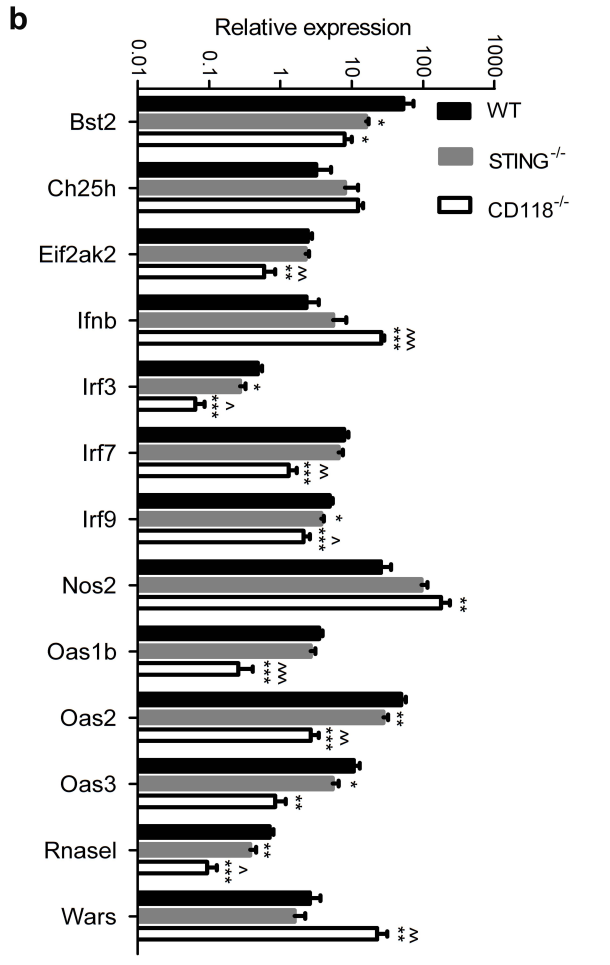
b
Relative expression
0.01
0.1
1
10
100
1000
WT
STING-/-
CD118-/-
Bst2
Ch25h
Eif2ak2
Ifnb
Irf3
Irf7
Irf9
Nos2
Oas1b
Oas2
Oas3
Rnasel
Wars

# Figure 3

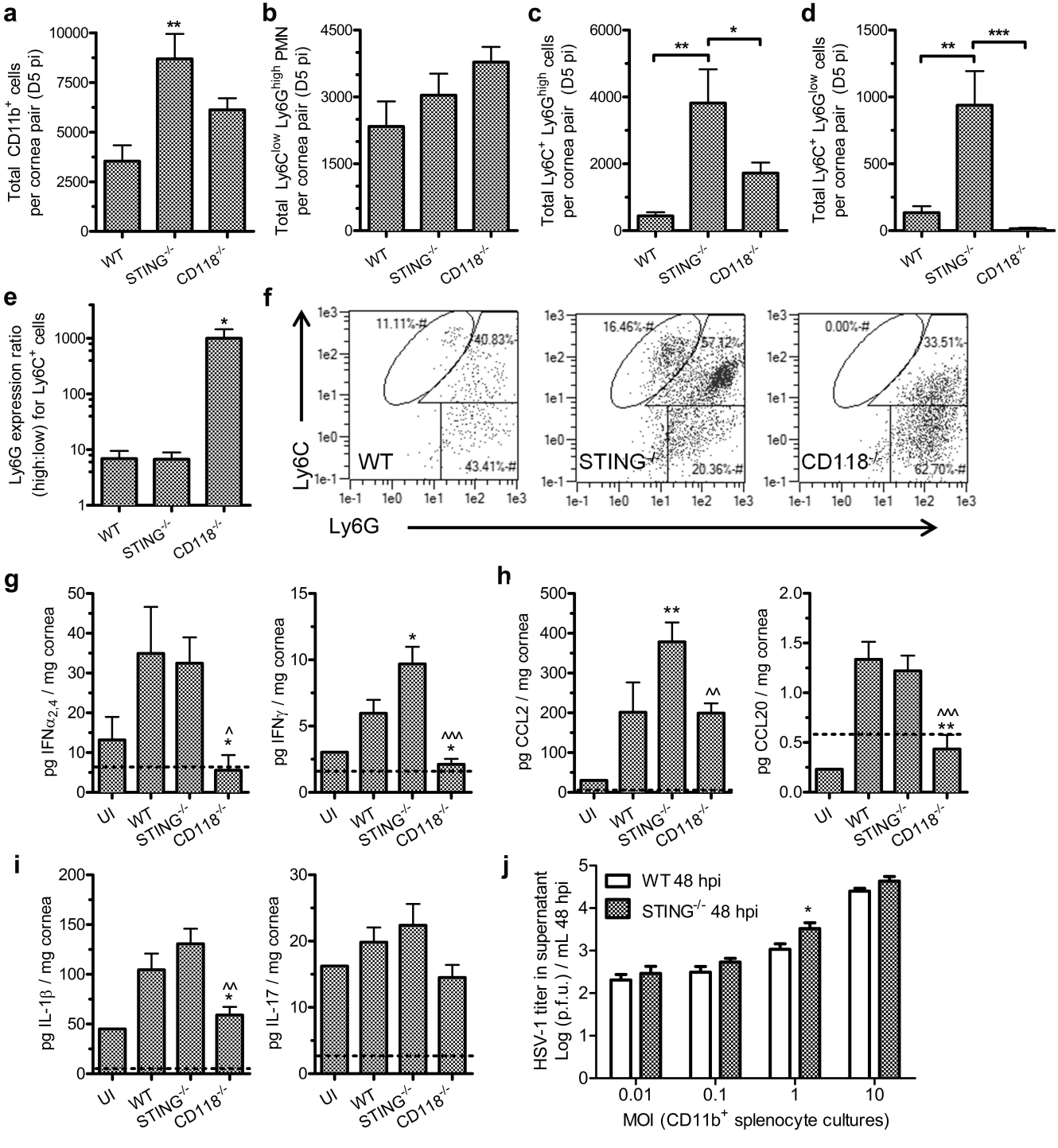
a
Total CD11b+ cells per cornea pair (D5 pi)
10000
7500
5000
2500
0
**
WT
STING-/-
CD118-/-
b
Total Ly6Clow Ly6Ghigh PMN per cornea pair (D5 pi)
4500
3000
1500
0
c
Total Ly6C+ Ly6Ghigh cells per cornea pair (D5 pi)
6000
4000
2000
0
**
*
d
Total Ly6C+ Ly6Glow cells per cornea pair (D5 pi)
1500
1000
500
0
**
***
e
Ly6G expression ratio (high:low) for Ly6C+ cells
1000
100
10
1
*
f
Ly6C
Ly6G
WT
STING-/-
CD118-/-
11.11%-#
40.83%-#
43.41%-#
16.46%-#
57.12%-#
20.36%-#
0.00%-#
33.51%-#
62.70%-#
1e3
1e2
1e1
1e0
1e-1
g
pg IFNα2,4 / mg cornea
pg IFNγ / mg cornea
UI
WT
STING-/-
CD118-/-
h
pg CCL2 / mg cornea
pg CCL20 / mg cornea
i
pg IL-1β / mg cornea
pg IL-17 / mg cornea
j
HSV-1 titer in supernatant Log (p.f.u.) / mL 48 hpi
WT 48 hpi
STING-/- 48 hpi
MOI (CD11b+ splenocyte cultures)
0.01
0.1
1
10

# Figure 4

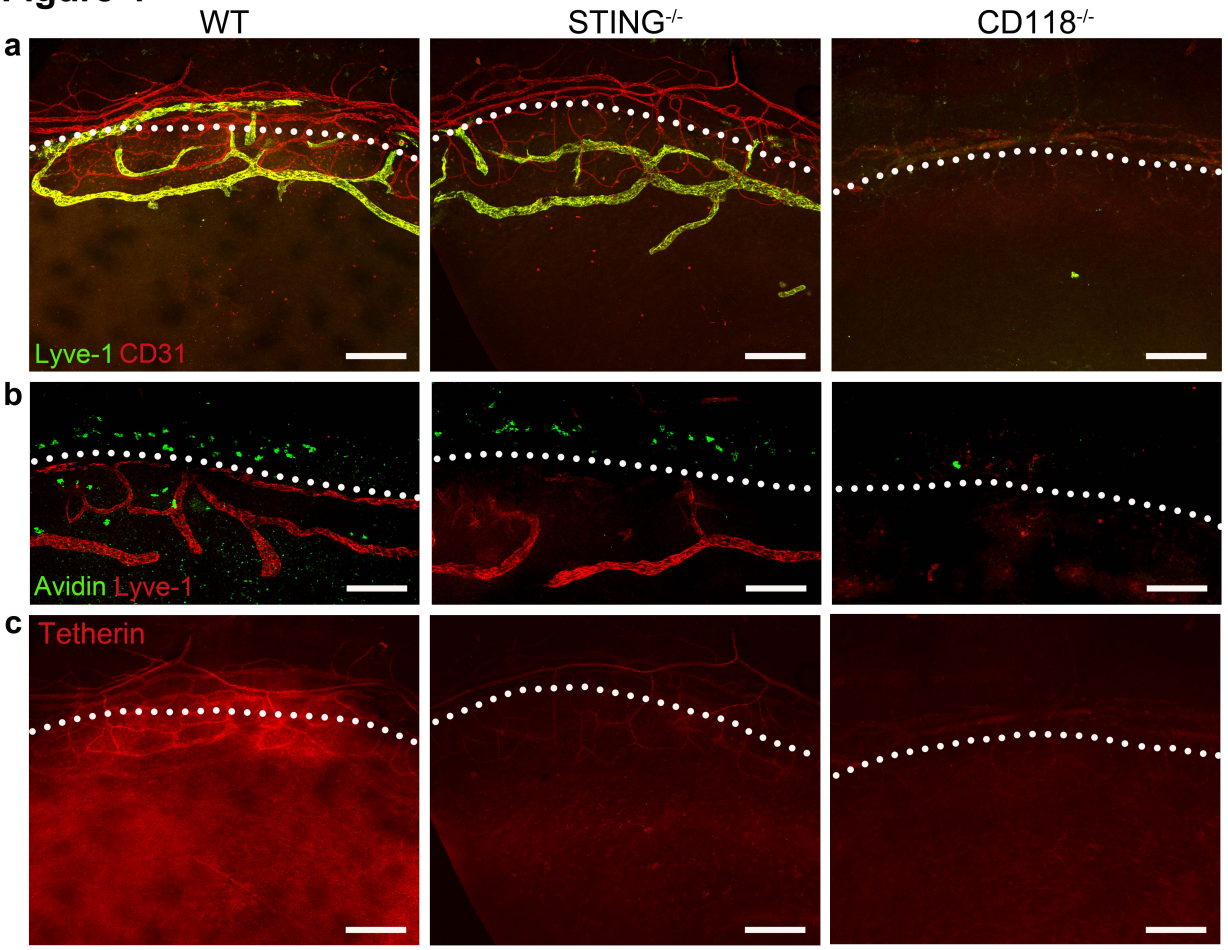

# Figure 5

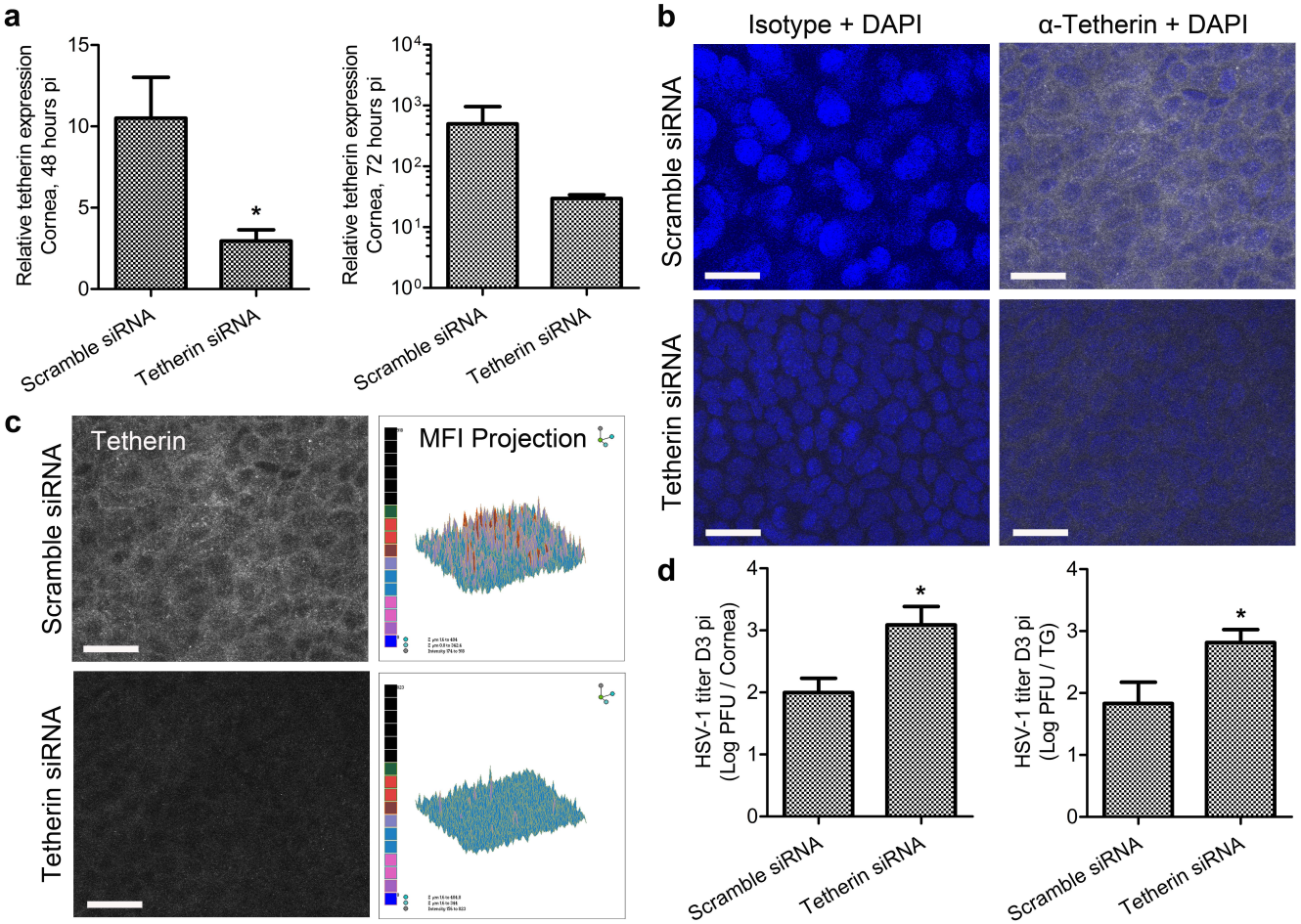
a
Relative tetherin expression
Cornea, 48 hours pi
15
10
5
0
*
Scramble siRNA
Tetherin siRNA
Relative tetherin expression
Cornea, 72 hours pi
10^4
10^3
10^2
10^1
10^0
Scramble siRNA
Tetherin siRNA
b
Isotype + DAPI
α-Tetherin + DAPI
Scramble siRNA
Tetherin siRNA
c
Tetherin
MFI Projection
Scramble siRNA
Tetherin siRNA
d
HSV-1 titer D3 pi
(Log PFU / Cornea)
4
3
2
1
0
*
Scramble siRNA
Tetherin siRNA
HSV-1 titer D3 pi
(Log PFU / TG)
4
3
2
1
0
*
Scramble siRNA
Tetherin siRNA

# Supplemental Figure 1

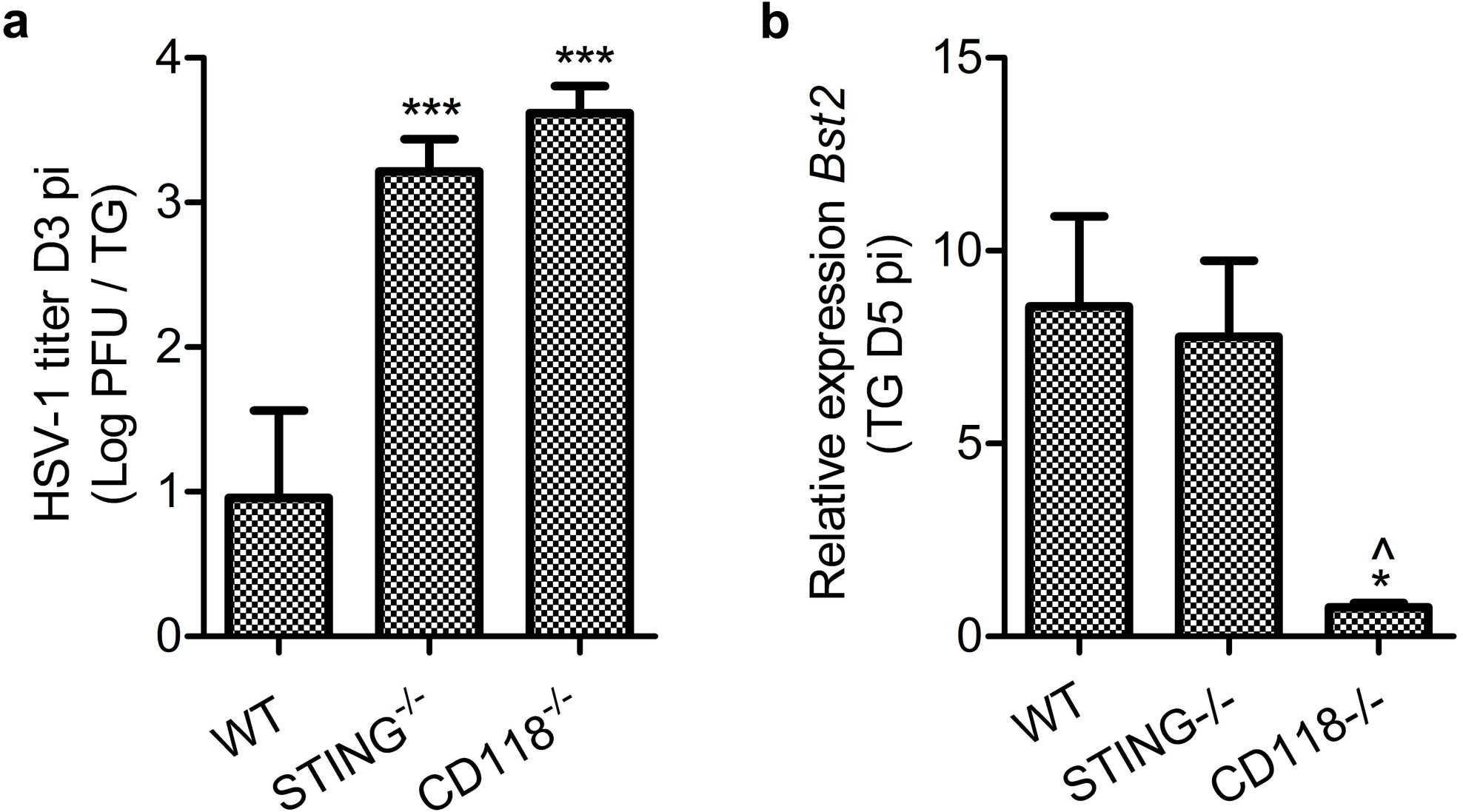

# Supplemental Figure 2